Increasing the Solar Share in Combined Cycles through Thermochemical Energy Storage

C. Ortiz, [a,*] R. Chacartegui [b], J.M. Valverde [c], A. Carro [b], C. Tejada [bd] and J.S. Valverde [bd]

[a] Universidad Loyola Andalucía, Av. de las Universidades s/n, Dos Hermanas, 41704 Sevilla, Spain
[b] Dpto. Ingeniería Energética. Universidad de Sevilla, Camino de los Descubrimientos s/n, 41092 Sevilla, Spain
[c] Facultad de Física, Universidad de Sevilla, Avenida Reina Mercedes s/n, 41012 Sevilla, Spain
[d] VirtualMechanics, S.L., c/ Arquitectura 1, 41015 Sevilla, Spain

[*] Corresponding author: cortiz@uloyola.es (+34) 655783930

Abstract

The integration of Concentrating Solar Power (CSP) in combined cycles is a subjects of increasing attention. Combined cycles require high temperature at the gas turbine inlet (typically over 1000ºC), which would hinder plant operation in the absence of direct solar radiation using currently commercial storage technologies based on molten salts (with a temperature limit around ~600ºC). Thus, solar power share in current Integrated Solar Combined Cycles (ISCC) is typically lower than 20%, while most of the thermal power required is provided by natural gas. The present manuscript proposes the integration of a Thermochemical Energy Storage (TCES) system based on the Calcium-Looping process, which can release the stored energy at temperatures above 1000ºC. The storage charging step uses the heat provided by a CO_2 stream previously heated in a high-temperature solar receiver. The configuration of the solar receiver-calciner is fundamental to determine the amount of storable energy. Results from the conceptual model simulation predict overall plant efficiencies above 45% (excluding solar side losses), suggesting a high potential for the development of this novel integration that would allow enhancing the solar share in combined cycles.

Keywords

Thermochemical Energy Storage, Dispatchability, Solar Energy, Combined Cycle, Calcium-Looping, Capacity Factor

1. Introduction

Concentrating Solar Power (CSP) is a promising technology to increase the energy storage capacity from renewables. The main current research lines for a successful deployment of CSP plants are [1]: i) increasing plant efficiency; ii) Levelized Cost of Electricity (LCOE) reduction; iii) increasing dispatchability and iv) improving sustainability and environmental impact. High-efficiency and sustainable power blocks are required for future high-performance CSP plants. An attractive option to increase efficiencies based on already known technology is to integrate the CSP system with a Combined Cycle (CC), which is the subject of the present investigation. In the so-called Integrated Solar Combined Cycles (ISCC), due to the high temperature required at the gas turbine, CSP is still considered to cover a small share of the thermal power required for the power block. Conlon [2] proposed a novel integration in which solar thermal was integrated by means of a medium temperature Thermal Energy Storage (TES) system to provide efficient heat to a Combined Cycle, allowing a higher dispatchability than in

traditional CSP plants. However, to further improve the solar contribution in combined cycles, the integration of novel thermal storage systems able to release the stored energy efficiently at high temperatures (>900ºC) should be sought.

Among the different TES alternatives capable of operating at high temperature, Thermochemical Energy Storage (TCES) systems are notably gaining momentum for this purpose. TCES uses solar energy to drive an endothermic reaction that breaks chemical bonds of a compound. The resulting products are stored. Under demand, the reaction products are brought together, to deliver heat through the reversible exothermic reaction. Nevertheless, TCES is yet in an incipient development stage. Several TCES systems are being proposed from computational simulations, laboratory tests and small-scale pilot plants [3]. Among the reactions proposed as TCES are those based on carbonates (i.e. $CaCO_3$ [4], $SrCO_3$ [5]), hydrides (i.e. MgH_2 [6]), hydroxides (e.g. $Ca(OH)_2$ [7], $Mg(OH)_2$ [8]), metal redox (e.g. Co_3O_4 [9]), organic compounds (i.e. CH_4 [10]), ammonia [11] and sulfur [12].

The calcium looping (CaL) process, based on calcination/carbonation of $CaCO_3$ (Eq.1) is one of the most promising TCES due to its high turning temperature, high energy density and the low price and full availability of the raw material (natural limestone or dolomite) [13]. Currently, the ambitious projects SOCRATCES [14] is developing a kW-scale prototype aiming to demonstrate the feasibility of the CSP-CaL integration and to reduce risks facing the scale-up [15].

$$CaCO_{3(s)} \rightleftarrows CaO_{(s)} + CO_2 \qquad \Delta H_r^0 = 178 \frac{kJ}{mol} \tag{1}$$

The idea of using the CaL process as TCES was early proposed by Baker in 1974 [16] and many works since then have been published on the conceptual integration of the CaL process in CSP plants [13] mainly based in the design and lab-scale testing of Ca based materialsto enhance the multicycle CaO activity (e.g. [17]) and in process integration [18,19]. Chacartegui et al. [4] firstly proposed the integration of a closed-CO_2 Brayton cycle to use the high-temperature released heat in the carbonation reaction. Ortiz et al. [20] proposed a simple integration between the power block and the carbonator to run a combined cycle. Other authors have considered the integration of steam or supercritical CO_2 cycles [21]. The novelty of the present work consists of a conceptual modelling approach to use in Solar Combined cycles the high-temperature energy storable by the CaL process. To tackle the current uncertainty of the operation of solar particle receivers under the specific reaction conditions, this work proposes novel indirect calciner where a pressurised gas stream (CO_2 in a first approach) is heated in a cavity receiver and used as Heat Transfer Fluid (HTF) to drive the calcination reaction.

Briefly, the proposed High-Temperature Storage Solar Combined Cycle (HTSSCC) works as follow: CO_2 (HTF) heated in a gas pressurised receiver transfers the heat for calcination to take place afterwhich is passed through a typical CC pathway. The calcination products (CaO and CO_2) are stored. At sunset, the stored CO_2 is sent to another CFB reactor where the exothermic carbonation of the CaO releases the stored heat to continue heating the HTF circulating through the combined cycle without solar input. A model has been developed for simulating the proposed plant. The results predict power cycle efficiencies above 45% (excluding solar side losses), which suggests a potential

usefulness of this integration to improve both the solar-to-electric efficiency and the capacity factor of CSP plants.

The paper is structured as follows: firstly, the current state-of-the-art of Integrated Solar Combined Cycles (ISCC) is discussed to highlight the relatively poor contribution of solar energy in these cycles. The current research lines to address this issue are described. Later, the novel cycle proposed in this work is explained in detail and simulated. Several receiver-calciner configurations are assessed due to their relevance on the amount of storable energy. Finally, the use of air and Helium instead of CO_2as potential HTF in the cycle is addressed.

2. State of the art of Integrated Solar Combined Cycles (ISCC)

Most of the fundamental research and industrial projects on solar combined cycles are based on ISCC configurations, where the integration of solar energy in the combined cycle aims to reduce fossil fuel consumption while maintaining high thermoelectric efficiency. However, industrial-scale ISCC plants possess a minor solar share, which is computed as the ratio between the solar-based energy production to the total energy produced by the power cycle.

Table 1 shows a summary of the main projects developed to date.

Table 1. Integrated Solar Combined Cycle (ISCC) projects worldwide

Name	Solar Technology (*)	Power (MWe)	Solar share (%)	Storage	HTF
Agua Prieta II	PT	478	2.9%	no	Thermal Oil
City of Medicine Hat	PT	203	0.5%	no	Thermal Oil
Ain Beni Mathar	PT	470	4.3%	no	Thermal Oil
Duba 1	PT	605	7.1%	no	Thermal Oil
Hassi R'mel	PT	150	13.3%	no	Thermal Oil
Kuraymat	PT	140	14.3%	no	Thermal Oil
Martin Next Generation SEC	PT	1150	6.5%	no	Thermal Oil
Waad Al Shamal	PT	1390	3.6%	no	Thermal Oil
Dadri ISCC	LF	210	6.7%	no	Water

(*) PT: Parabolic Trough; LF: Linear Fresnel

Waad Al Shamal ISCC Plant, currently under construction, is so far the biggest plant, with a total output of 1,390 MWe (4 gas turbine + 1 steam turbine), of which 50 MW correspond to the CSP plant. Smaller ISCC plants as Hassi R'mel and Kuraymat have larger solar shares albeit yet small (13-14%). As shown in Table 1, the solar share is not significant from a power production perspective, and the operation of these plants do not differ much with the availability of the solar resource. Some of these plants, as in the case of Agua Prieta II ISCC, have additional natural gas duct–burner (14 MWe) allowing the same energy generation in the absence of solar. As can be seen in Table 1, a common factor for the ISCC concept is the nonexistence of storage, which notably limits the solar share to the total energy produced throughout the year.

In recent years, many innovative integrations are being proposed to improve the CSP thermal integration in combined cycles and therefore, the solar share in these plants [22]. Table 2 shows a summary of selected published works on ISCC.

Table 2. Published works in ISCC

Ref.	Solar Technology-integration (*)	HTF (**)	Solar integration (***)	Solar share (%)	Tmax solar (ºC)	Storage (hours)	Design efficiency (%)
[23]	PT	TO	EV	41.0%	450	no	57
[24]	PT	TO	EV	37.3%	-	no	42.8
[24]	PT	TO	PH/EV	39.4%	-	no	33.7
[24]	PT	TO	EV/SH	37.3%	-	no	42.8
[24]	PT	TO	PH/EV/SH	39.4%	-	no	32.6
[24]	PT	DSG	EV	38.4%	-	no	44.6
[24]	PT	DSG	PH/EV	42.5%	-	no	32
[24]	PT	DSG	EV/SH	34.7%	-	no	45.7
[24]	PT	DSG	PH/EV/SH	37.9%	-	no	37.8
[25].	PT	TO	EV	23.7%		no	54.1
[25].	PT	DSG	EV	27.8%	300	no	53.4
[26]	PT	DSG	EV	5.7%	566	no	-
[27]	PT	TO	EV	24-27%	371	no	-
[27]	CR	MS	SH	30-41.5%	538	no	-
[27]	LF	DSG	SH	30-41.5%	500	no	-
[27]	CR	DSG	SH	30-41,5%	565	no	-

(*) PT: Parabolic Trough; LF: Linear Fresnel; CR: Central Receiver.
(**) TO Thermal Oil; MS: Molten salts; DSG: Direct Steam Generation
(***) EV: evaporator; SH: superheater; PH: preheater.

The most commonly used solar thermal technology is the parabolic trough with a solar share between 30-40% (Table 2). Thermal oil and DSG configurations are employed, both in the parabolic trough and central receiver, incorporating the solar contribution to different points in the HRSG. None of these studies make use of energy storage to improve the solar share throughout the year operation.

3. A novel concept for a solar combined cycle with energy storage

The present work proposes a novel High-Temperature Storage Solar Combined Cycle plant with the potential to notably improve the peak plant efficiency and the capacity factor of CSP plants. The process is developed from the integration of solar energy at high temperature (1000ºC) in a closed combined cycle. A high-temperature TCES system based on the CaL process is proposed to improve the capacity factor of the plant. The incorporation of the TCES system is a relevant novelty of this work in comparison with previous investigations. It allows a notably increase of solar share in combined cycles, extending the contribution of the solar resource to periods where it is not available (i.e. at night) reducing the need for fossil fuel. The HTSSCC conceptual plant proposed in this work has the potential to operate without fossil fuel back-up, with a 100% solar contribution. Facing the potential scale-up of this concept a natural gas back-up could be incorporated to heat the HTF at the gas turbine inlet, to ensure stable gas turbine operation during solar transients or to optimise power plant sizing and cost [28], and therefore minimising operation risks of the novel CSP-TCES system.

Figure 1 shows the conceptual scheme of the proposed integration. Two well-differentiated operation modes are considered: sun and night modes. CO_2, which is used as Heat Transfer Fluid (HTF), is compressed and sent to a high-temperature cavity

receiver through SiC tubes, where it is heated up to temperatures around 1200ºC (s1 in Figure 1). At this temperature the HTF provides thermal power for the calcination reaction to take place at 950ºC, while it leaves the reactor at around 1000ºC ($\Delta T \sim 200$ºC) to enter the gas turbine. The calciner is a CFB reactor where the energy storage process starts. The endothermic calcination of $CaCO_3$ takes place at 950ºC in the calciner at atmospheric pressure under pure CO_2. Although the equilibrium temperature at these conditions is ~ 896ºC [29] (Figure 2), temperatures above 930ºC are necessary to achieve full calcination at a sufficiently fast rate [30].

CFB is a well-developed technology at the industrial scale. CFB based reactors to carry out calcination/carbonation of $CaCO_3$ have been shown to work effciently in the CaL process to capture CO2 [31,32] as these reactors ensure efficient gas-solid contact and heat/mass transfer. In the case of calcination, a certain amount of extra CO_2 from the storage tank would be recirculated to fluidized the $CaCO_3$ particles. Separation of the calcination products before storage is feasible using commercially available cyclones. The CaO produced is directly sent to another CFB reactor (carbonator), where it is stored at high temperatures. Carbonation of CaO solids would be carried out in a bed fluidized by CO_2 at high pressure [33]. The calciner and carbonator are typically operated under the fast fluidisation regime with gas velocities of the order of 5-10 m/s [34]. Alternatively, an intermediate CaO storage silo could be integrated to increase the storage capacity [4] and reduce the volume of the CFB reactors [35]. A high-temperature pneumatic conveying system would be required in this case to feed the carbonator at sunset. The CO_2 released in the calciner has to be cooled before compressing. To take advantage of its high temperature, it is passed through a packed-bed tank filled with steel slag to charge a high-temperature energy storage system. Steel slag has been previously proposed as an efficient TES at temperatures as high as 1000ºC [36], with high potential to be integrated into CSP plants due to its high thermal conductivity, heat capacity, and low cost [37]. A similar CO_2 TES system, but considering ceramic particles instead of steel-slag, was proposed by Peng et al. [38]. Once the CO_2 sensible heat is recovered, the stream is compressed at high pressure (75 bar), cooled, and stored at 25ºC to guarantee a reduced specific volume at liquid phase [4]. An intercooled CO_2 compression (4 stages) is employed to reduce the overall power consumption [4].

Following the description of the process (Figure 1), the solar receiver in the base case has a net power capacity of 430.6 MWth to guarantee 100 MWth stored at the calciner under design conditions. Preliminary estimates suggest a receiver efficiency of ~60-70% due to the radiation losses at those temperatures. A three-cavity receiver is considered to cover a 360º heliostats field [39]. Inside the cavity, the HTF (CO_2) passes through a set of pressurised tubes absorbing the solar radiation. These tubes could be made of SiC [40] or a nickel-based alloy (Inconel 617), as in the case of the solar receiver at the SOLUGAS project (4.7 MWe), where compressed air was heated from 330ºC to 800ºC. In SOLUGAS, the design consisted of 10 circular arranged panels, each one equipped with 17 Inconel absorber tubes of 5m radiated length [28]. Because of the high temperature (1200ºC), a cavity design that minimises radiation losses plays a key role in the overall plant performance. Receiver efficiencies around 80% were achieved at the SOLUGAS facility.

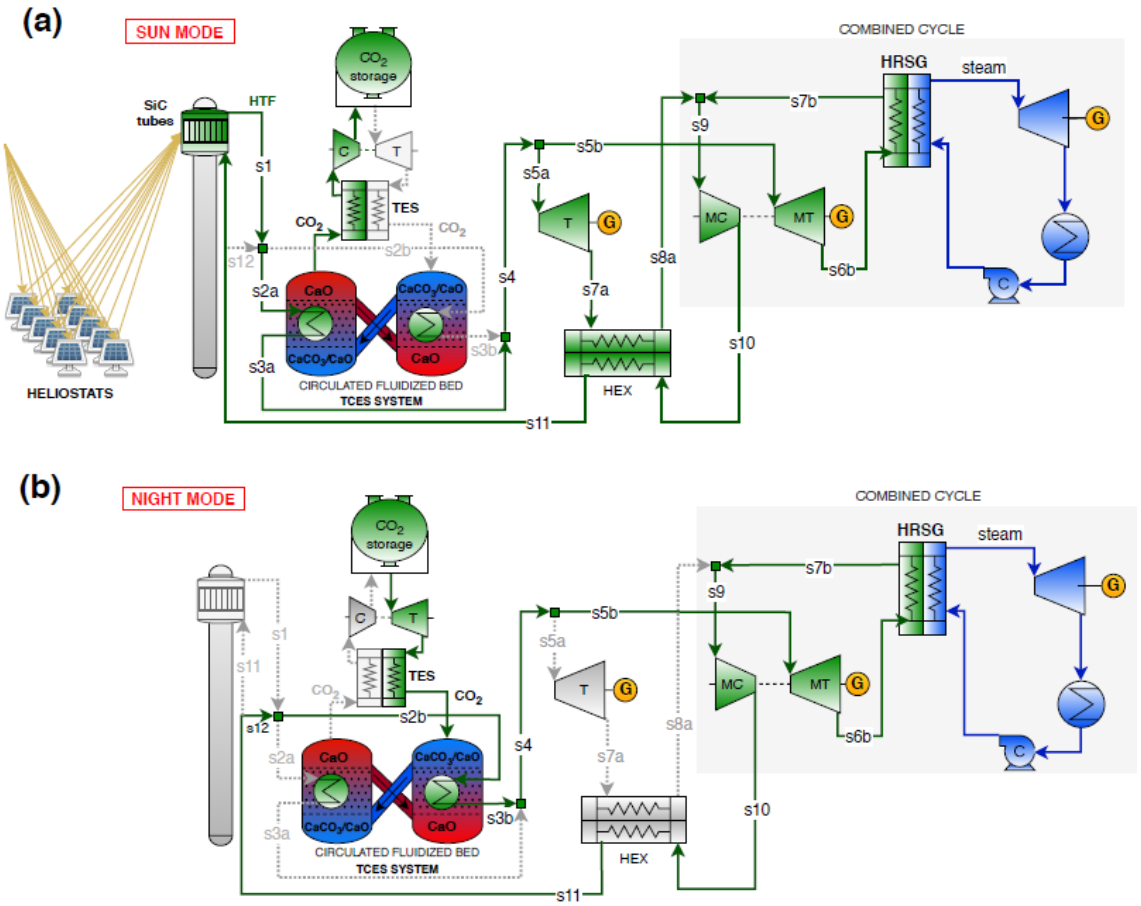

Figure 1: Conceptual scheme of the novel HTSSCC plant; a) operation under 'sun ' mode'; b) operation under 'night ' mode'. Note that streams and equipment in grey colour are not used in each respective mode.

At the CFB reactor exit (s3a), the HTF at 1000ºC is expanded in two parallel turbines (T and MT in Figure 1a) up to atmospheric pressure. A Pressure Ratio (PR) of 18 has been chosen at the design point, with near-to-atmospheric pressure at the turbine outlet. This selection has been carried out from a sensitivity analysis to optimise power production as a function of the PR (see Figure 7). The HTF stream exiting the turbine T (s7a) passes through a gas-gas heat exchanger to release sensible heat before being compressed and resent to the solar receiver. At the turbine MT exit, the HTF (s6b) passes through an HRSG in a typical closed combined cycle path. A triple-pressure reheat steam cycle is used as a bottoming cycle, with live steam conditions of 100 bar and 550ºC, similar to other Rankine cycles integrated into solar tower-based plants [41]. For a new cycle, the HTF stream is recompressed (s10) and preheated before entering the solar receiver up to ~450ºC, which is the maximum temperature reachable under the design conditions. This allows a reduction of thermal stresses due to temperature gradients in the receiver. As a novelty over typical fuel-based combined cycles, intercooling compression serves to significantly enhance the plant performance under the 'sun mode' operation. In the proposed configuration, the HTF exiting the compressor (at around 100ºC due to the cooling stages) is preheated before entering the solar receiver (HEX in Figure 1). Intercooling stages notably reduce the compression work required [42]. However, this inter-cooling compression is not beneficial at the 'night' operation mode, in which HTF is directly sent from the compressor (MC) to the CFB carbonator. Thus, for improving the

overall plant operation, cooling is activated when compressing under the 'sun' mode (Figure 1a) and deactivated at 'night' mode (Figure 1b).

At sunset, the 'night mode' operation is activated Figure 1b), and the thermal energy to drive the power block (gas turbine + bottoming steam cycle) begins to be transferred from the carbonator CFB reactor. It is imposed as a design criterion to maintain the same Turbine Inlet Temperature (TIT) than in the sunshine hours. Therefore, carbonation occurs under pure CO_2 at 1000ºC and 8 bar. At this pressure, the equilibrium temperature is ~1070ºC (Figure 2) but the carbonation temperature cannot be too close to the equilibrium temperature to avoid extremely low kinetics [43]. Ideally, both the calcinaton and carbonation reactions must occur fast enough to be fully achieved before the particles leave the reactors. Calcination and carbonation kinetics analyses are out of the scope of this work. Thus, in the steady-state simulation it is assumed that carbonation of CaO occurs for the typical residence time in CFB reactors (2-10 minutes) up to the residual value measured in multicycle TGA tests [44,45]. Likewise, calcination kinetics under the proposed conditions is expected to occur in less than 5 minutes [46].

The small temperature difference between calcination (950ºC) and carbonation (1000ºC) allows an efficient thermal integration heat recovery without the need of using expensive solid-gas heat exchangers [47]. Thus, the CaO exiting the calciner is introduced in the carbonator, where it is stored until energy generation is needed. To avoid unwanted energy release in the carbonator when the plant is powered by solar energy, carbonation should be avoided until the control system orders the generation of energy from the stored CaO. This can be done by keeping the reactor pressure below the equilibrium pressure (see Figure 2). Therefore, once the carbonation is finished at the end of the 'night' operation mode, the carbonator must be depressurised.

The 'night mode' starts from the CO_2 stored, which is preheated while passing through the steel slag-based TES before being expanded from 75 bar (storage pressure) to 8 bar (carbonation pressure) and before entering the carbonator. In the CFB carbonator, CO_2 reacts with the bed of CaO to regenerate the $CaCO_3$ through the carbonation reaction (Eq. 1), releasing the stored heat. One drawback of the CaL process is the progressive loss of CaO carbonation activity as the number of cycles increases mainly due to CaO grains sintering [48] or pore-plugging [17], depending on calcination/carbonation conditions and the CaO precursor used [13]. Thus, only a fraction X of the total flow of CaO entering the carbonator reacts to produce $CaCO_3$, while $1\text{-}X$ remains as unreacted CaO. As shown from TGA tests the multicyclic CaO conversion decays until it reaches a residual conversion value (Xr), which depending on the process conditions can vary within a wide range (Xr=0.07-0.82) [13]. CaO deactivation plays a key role in the CaL process performance [13] and could be partially compensated by the periodic introduction of fresh limestone makeup. The purged CaO is particularly well suited for cement production [49]. In the present work, a conservative value of Xr=0.15 is assumed. The energy density of entire systems highly varies depending on CaO conversion due to the larger amount of solids to be stored due to incomplete conversion thereof [33].

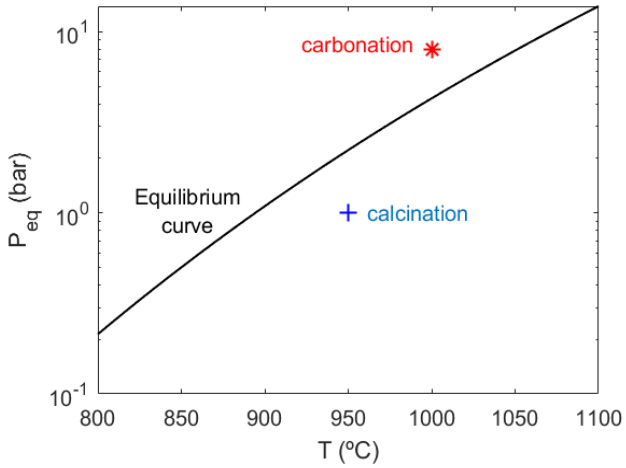

Figure 2: Calcination-carbonation temperature and CO_2 pressure proposed for plant operation.

Once carbonation begins, the compressed HTF (s12 in Figure 1b) enters the CFB carbonator, instead of entering the solar receiver, where is heated indirectly by the heat released in the reaction. Later, the HTF is expanded (MT) and passes through the HRSG (steam bottoming cycle) as in the 'day' mode before being compressed again. Thus, the combined cycle (MC/ MT and steam cycle) has the potential to work 24h with the same power output, being the thermal power provided either by the solar or the TCES systems.

3.1 Conceptual model of the plant

A model of the solar power plant integration performance has been developed to evaluate the potential of the novel concept under design conditions. This model has been developed within the commercial software Thermoflex® and Aspen Plus®. As a first approach, this work considers steady-state operation over the whole day: 12h of constant solar input (sun mode) and 12h without solar input (night mode). Further research considering real solar patterns, off-design efficiencies, operation strategies, and annual plant performance will be carried out in future work. All the processes are steady-state and steady flow. As a design criterion, the Solar Multiple (SM) is calculated to provide constant electric power in the combined cycle (MC-MT and steam turbine) along the whole day. Under this simplified approach, plant efficiency is determined as an average of the performances in the 'sun' and 'night' modes (Eq.2) [33]:

$$\eta = \frac{\int_{24h} \dot{W}_{net}\, dt}{\int_{24h} \dot{Q}_{input}\, dt} = \frac{\dot{W}_{net,sun}\, \Delta t_{sun} + \dot{W}_{net,night}\, (24 - \Delta t_{sun})}{\dot{Q}_{input}\, \Delta t_{sun}} \quad (2)$$

Where $\dot{W}_{net,sun}$ and $\dot{W}_{net,night}$ are the net power produced in 'sun' and 'night' modes, respectively, Δt_{sun}=12h and $\dot{Q}_{input}$ is the net solar power to the powerplant. Solar-side losses (solar field and receiver) are not considered, and therefore Eq.2 does not refer to solar-to-electric efficiency.

Table 3 summarises the main assumptions made in the reference model. Values for the selected parameters are chosen based on literature or commercial equipment data. A

sensitivity analysis is carried out in the next section to analyse the effects of some of these parameters over the plant efficiency.

Table 3: Main assumptions in the reference model (see Figure 3)

Group	Parameter	Component	Value
CO_2 turbomachinery	Isentropic efficiency	PB Turbines/compressors	0.91
	Mechanical efficiency	Turbines/compressors	0.99
	Intercooling/reheating	Main Compressor (MC)	2 stages (20ºC)
		CO_2 compressor (C)	4 stages (40ºC)
		CO_2 turbine (T)	3 stages (100ºC)
Pumps	Isentropic efficiency	All	85%
	Mechanical efficiency	All	99%
Steam turbine	Pressure losses	Steam pipes	2%
	Group Efficiency	HPT	77%
		IPT	88%
		LPT	90%
Generator	Efficiency	Gas turbine	99%
		Steam turbine	98%
Reactors	HTF pressure losses	carbonator/calciner	2%
	conversion	calciner	100%
		carbonator	15%
	HTF thermal effectiveness	carbonator/calciner	95%
Storage Vessels	Thermal losses	CO_2 storage, CFBs	0%
Heat exchangers	Pressure drop	HEX	1%
		HPS	2%
		LPS, IPS	6% (water)
		HEP2, HEP1, ECO	2% (water)
	Blowdown	HPB, IPB, LPB	1%
	Design Pinch	HPB, IPB, LPB	10ºC
	Minimum pinch	All steam cycle	5
	Thermal effectiveness	HEX	95%
		TES	95%
	Normalised heat losses	All	1%
Receiver	Pressure losses	-	2%

Turbines are modelled just from a thermodynamic perspective providing an adiabatic expansion. CO_2 properties are taken from REFPROSP (NIST) database, whilst IFC-67 is used for steam properties formulation. Table 3 details all the efficiencies assumed in the Thermoflex and Aspen Plus models. A water-intercooled compression is considered in the main compressor under 'sun mode', whilst under 'night mode' intercooling is avoided. An identical compressor stage isentropic efficiency is used to compute the compression work for each stage. A condensing, single reheat steam turbine cycle is considered with a typical casing configuration divided into High-Pressure Turbine (HPT) and Intermediate (IMT)/Low Pressure Turbines (LPT). For simplicity the heat transfer process in TCES and TES systems is simplified by assuming thermal effectiveness, which is used by the model to calculate the heat transfer between the two streams. Effectiveness is defined as the ratio of the actual heat transfer rate to the maximum value that would be transferred by a counterflow heat exchanger of infinite size with zero losses [50]. Temperature profiles produced for these heat exchangers reflect any distinct changes in the specific heat of each of the fluids. Within the HRSG unit, more than one zone of heat transfer is considered (see TQ diagram in Figure 4), and the overall heat exchange capability of the heat exchanger, UA, is determined as the sum of the UA values of each zone. The condenser is simulated as a counterflow heat exchanger. Heat exchangers inside the storage systems are assumed to be large enough to achieve a given heat transfer. According to Ortega et al. [37], thermal efficiency of 95% could be reached in steel slag packed-bed tanks. Further detailed modelling is required to estimate tank sizes. No thermal loss in the storage system is considered at this stage, but it should be considered in a more detailed model considering the operation throughout the year. Due to the high

temperature of these storage systems, thermal insulation is required to minimise heat losses. Miller et al. [51] proposed a novel thermal energy insulation for high-temperature (>1000ºC) storage tanks. For a high-temperature TCES/TES at 1000ºC hourly energy losses would be 0.18% [38].

4. Process simulation and results

The proposed reference plant has been simulated at design conditions for each operation mode. Table 4 summarises the main input parameter for the base case. All the equipment and process streams are shown in Figure 3. A detailed description of each stream is presented in table A1 (Annexes).

Table 4: Main parameters used for simulating the HTSSCC plant at the design point

Group	Parameter	Value
Receiver	Net solar power	430.6 MWth
	Sunlight hours	12 h
Power block	TIT	1000ºC
	PR	18
	MT power	75 MWe
	Live steam conditions	550ºC, 100 bar
	Average (day-night) atmospheric conditions	15ºC, 60% RH
TCES	Average CaO conversion (X)	0.15
	Carbonator conditions	1000ºC, 8 bar
	Calcination conditions	950ºC, 1 bar
	CO_2 storage conditions	75 bar, 25ºC

The energy balance resulting from the base case simulation is shown in Table 5. Around 25% of useful solar heat at the receiver is transferred to the TCES system to carry out calcination. Due to the high temperature of the CO_2 exiting the calciner (C1), 7% of the solar input is stored as sensible heat. In the TES system, CO_2 cooling (charge) and heating (discharge) are almost identical (mass flow, temperature difference along with the tank) but separated in a time interval of several hours. It allows an optimum integration and use of the stored volume. Since no thermal losses are considered in the steel slag-based TES system, the system can transfer the heat taken from the hot CO_2 at the sunshine hours to the cold CO_2 released at sunset from the storage tank.

As shown in Table 5, power consumption and generation are higher under the 'sun' mode because of the need of circulating a larger quantity of HTF not only for power production but also for charging the storage system, whilst the net power production in the combined cycle is kept constant in both the 'sun' and 'night' modes (~52 MWe). Several strategies can be followed to control the HTF mass flow (and therefore power production) in a closed cycle such as including an HTF inventory, a bypass strategy or by a temperature control [52]. Regardig the control strategy based on a new HTF inventory, a well-insulated tank should be used to manage the different flow rate throughout the daily operation to avoid excessive thermal losses.

Power block efficiency under the sun mode (~32%) is penalised because of the charging step since a substantial amount of solar thermal power is stored and not used to generate electricity. Besides, charging extra energy consumption (9.56 MWe) occurs due to the necessary CO_2 compression up to the storage conditions (75 bar). On the other hand, operation under the night mode yields efficiency values of ~50% from the heat released

during carbonation. Figure 4 shows the T-S diagram for the HTF (CO_2) throughout the combined cycle and thermal integrations in the HRSG. Note that subcritical CO_2 conditions are considered (maximum pressure of ~18 bar). Figure 4b illustrates the three different heat exchanger zones in the HRGS. Most of the heat exchange with the steam occurs at high and medium pressure. A pinch-point ~10ºC is obtained while the HTF exits the HRSG at ~100ºC returning to the main compressor.

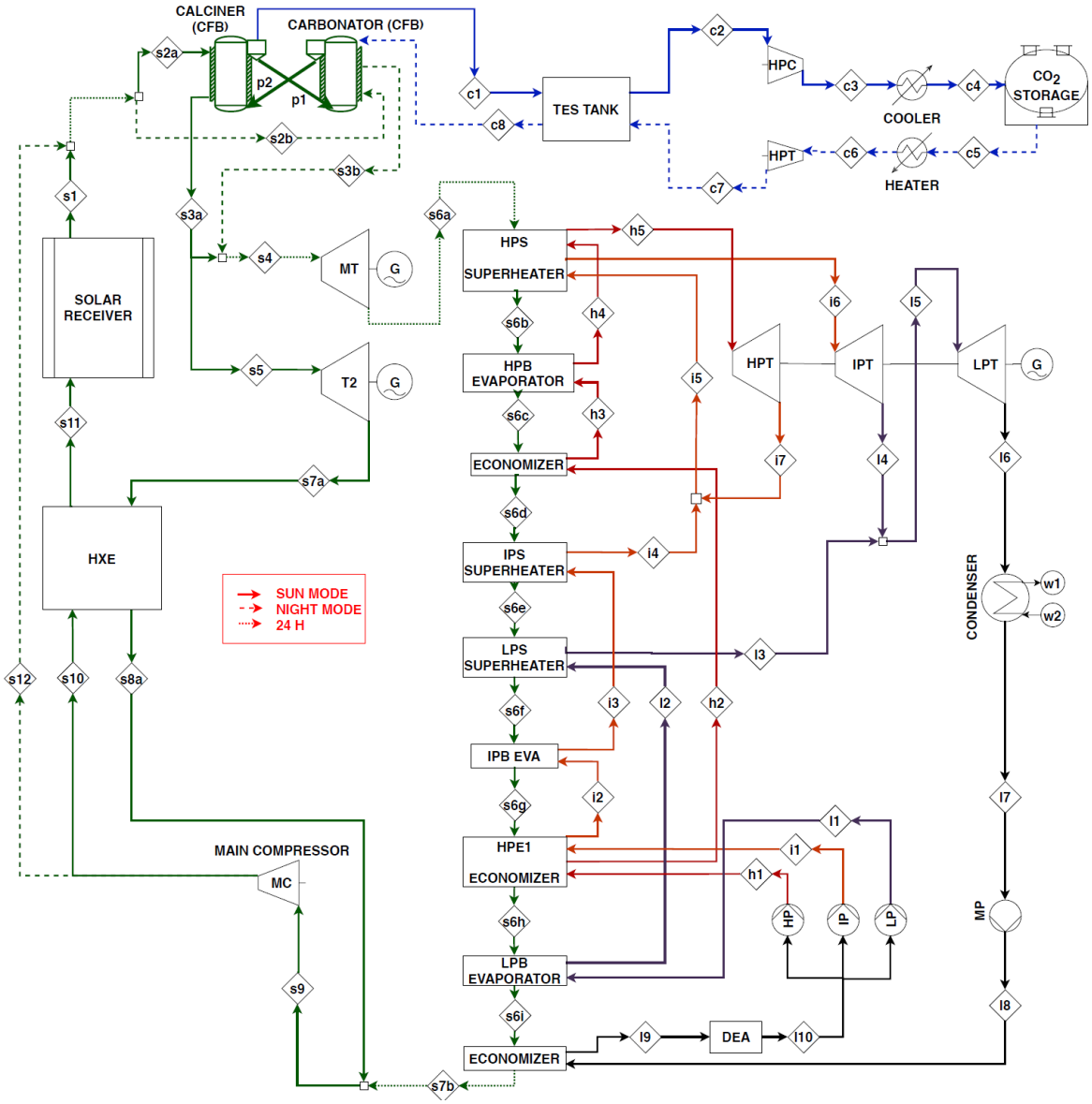

Figure 3: Detailed scheme of the HTSSCC plant (stream data for the base case is shown in table A1 -Annex section-)

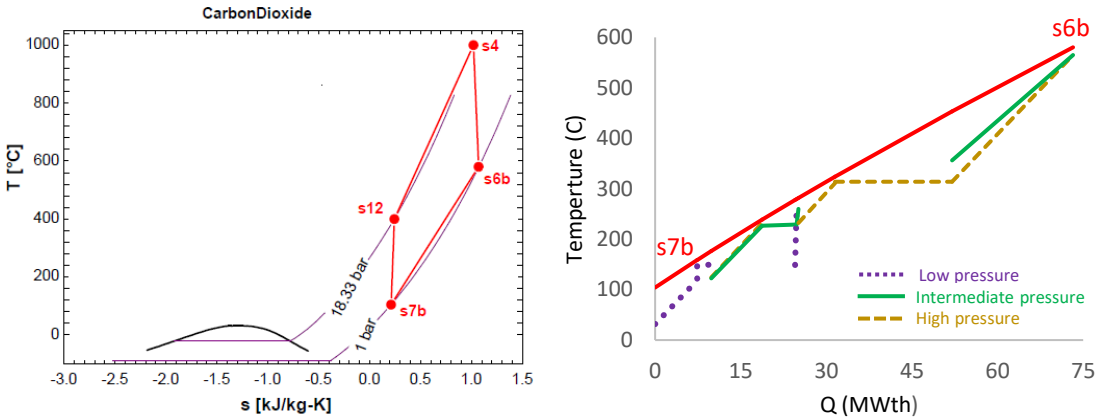

Figure 4: Combined cycle diagrams. a) T-S diagram of the HTF (CO_2) along the power block. b) Cumulative temperature-heat chart of the heat release in the HRSG.

Table 5: HTSSCC plant energy balance (base case)

	Parameter	Base case (Figure 3)	
		sun mode	night mode
	Solar thermal power (MW_{th})	430.6	0
Heat exchangers Thermal Power (MWth)	HXE	137.6	-
	CALCINER HE	115.0	-
	TES	41.3	39.2
	CO_2 COOLER	10.7	-
	CO_2 HEATER	-	7.9
	CARBONATOR HE	-	104.0
	HP-COMP (intercooler)	8.6	-
	TURB1 (interheater)	-	5.38
	MC (intercooler)	112.2	-
	HRSG	73.2	73.2
	CONDENSER	45.28	45.28
Power production (MWe)	Main HTF turbine (MT)	75.0	75.0
	HTF turbine (T2)	152.66	-
	Steam turbine (HPT)	4.87	4.87
	Steam turbine (IPT)	9.10	9.10
	Steam turbine (LPT)	13.88	13.88
	CO2 storage turbine (HPT)	-	3.77
Power consumptions (MWe)	Main HTF Compressor (MC)	-103.02	-47.26
	CO_2 storage compressor (HPC)	-9.56	-
	Steam cycle pumps (MP, LP, IP, HP)	-0.32	-0.32
	Cooling pumps/fans	-1.63	-0.59
	Miscellaneous auxiliaries	-2.64	-1.13
	Generators losses	-2.85	-1.30
Wnet	$\dot{W}_{net,sun}$	**135.49 MWe**	-
	$\dot{W}_{net,night}$	-	**56.02 MWe**
	Overall plant efficiency (η)	**44.5%**	

The HTSSCC yields an overall plant efficiency of 44.5%. This efficiency is higher than the reported by previous CSP-CaL integration works based on the direct integration of Closed Brayton cycles with low-temperature storage (~42% under the base case) [53], high-temperature storage (~38%) and by indirect integration of combine cycles (~40%). Note that none of these values for the overall efficiency considers solar-side losses.

4.1 Analysis of different integration alternatives

A key point on the design of dispatchable CSP systems is the selection of the storage size (usually referred by power block full operation hours at rated conditions) and the Solar Multiple (SM), which is the ratio of the receiver design thermal output to the power block design thermal input. SM 1 means that no thermal storage is used, and SM 3 means that 1/3 of the thermal power at the receiver is used in the power cycle while 2/3 are stored in the TES system for later use. The higher SM, the higher solar field cost and plant capacity factor [54]. According to the IRENA database [55], an SM 2.5 with 4h, 8h and 15h of TES leads to an annual capacity of 40%, 45% and 48% respectively. A design value of SM~1.5-3 is usually considered in CSP plants [54]. Remarkably, when considering CaL as an energy storage system, a higher SM leads to a lower plant efficiency mainly due to the higher CO_2 production in the calciner that has to be compressed [56]. This also occurs for other solid-gas TCES systems. In this section, four potential receiver-storage configurations (Figure 5) are proposed. A temperature difference between the HTF inlet/outlet at the calciner of 200ºC has been fixed for all cases.

As a novelty over a typical indirect molten salts-based TES system, the HTF temperature drop between the storage charging (1200ºC at the inlet and 1000ºC at the outlet of the CFB) and the discharge (~450ºC-1000ºC) is notably different, leading to a low SM and therefore a small energy storage capacity. Therefore, by circulating the HTF stream sequentially through the receiver, calciner and power block (case 2 in Figure 5b), the amount of thermal power provided to the solar receiver and calciner are, respectively, 187.5 MW and 37.9 MW at design conditions, which yields an SM of 1.25 (case 2 in Table 6). By considering the simplified sun and night operation modes, this leads to 4h full operation of the combined cycle (MC-MT-steam turbine) from sunset. In order to increase the storage capacity, the modification of the base case is proposed (Figure 5a). The HTF exiting the receiver at 1200ºC passes through the calciner (where it releases sensible energy) exiting at 1000ºC. Later, the HTF stream splits into two gas turbines with the same Pressure Ratio (PR). One of the streams is taken to the HRSG (in a typical combined cycle path) while the other is recirculated and used to preheat the HTF entering the receiver. The higher the amount of HTF recirculated, the higher the HTF temperature entering the receiver, and therefore, the lower the ratio solar thermal power/calciner thermal power. Under the design conditions, the system has a storage capacity able to provide 12h of power block full operation at design conditions, allowing under this simplified scenario a constant power production in the combined cycle along the whole day. Thus, the base case notably improves the plant capacity factor (dispatchability), although it involves a more complex configuration (including a new turbine regarding the case 1) and a sun mode efficiency two percentage points lower than in case 2.

Alternatively, in the configuration proposed as case 3 (Figure 5c), the HTF streams exiting the solar receiver splits before the calciner, which means that the Turbine Inlet Temperature (TIT) in the main turbine is increased to 1200ºC in the sun operation mode, while it continues

at 1000ºC (carbonator temperature) in the night mode. Gas turbines adapt to changes in operating temperature faster than the steam turbines [57], so the design criterion is to maintain temperature and pressure conditions of the HTF at the HRSG inlet throughout the day while varying the HTF mass flow between 'sun' and 'night 'operation modes. It involves working with different PR during the 'sun' mode (PR=55) than at night (PR=18 as in the base case). Therefore, the gas turbine stages should be appropriately sized.

After the calciner, the HTF stream is recirculated at high temperature and high pressure to the solar receiver by a fan. This configuration allows smaller temperature changes in the solar receiver (which leads to a remarkably smaller receiver size and minimises thermal stress inside it). The design is more straightforward than in the base case, avoiding a sizeable gas-gas heat exchanger and the second gas turbine. However, the plant efficiency is penalised by two percentage points regarding the sun operation mode in the base case (Table 6), and it is a more complex operation between day and night modes. To improve case 3 overall efficiency and operation, case 4 proposes an intermediate solar reheat stage in the main turbine (Figure 5d). At the first turbine exit (PR=3), the HTF is reheated up to 1000ºC before entering the second turbine (PR=18 up to near-to-atmospheric pressure at turbine outlet), which leads to an operation of the HRSG identical to the base case. As shown in Table 6, plant efficiency and storage capacity are improved, and operation can be simplified since the combined cycle (MT and steam turbines) works at the same conditions in both sun and night modes while the first turbine (see Figure 5d) can be by-passed at sunset.

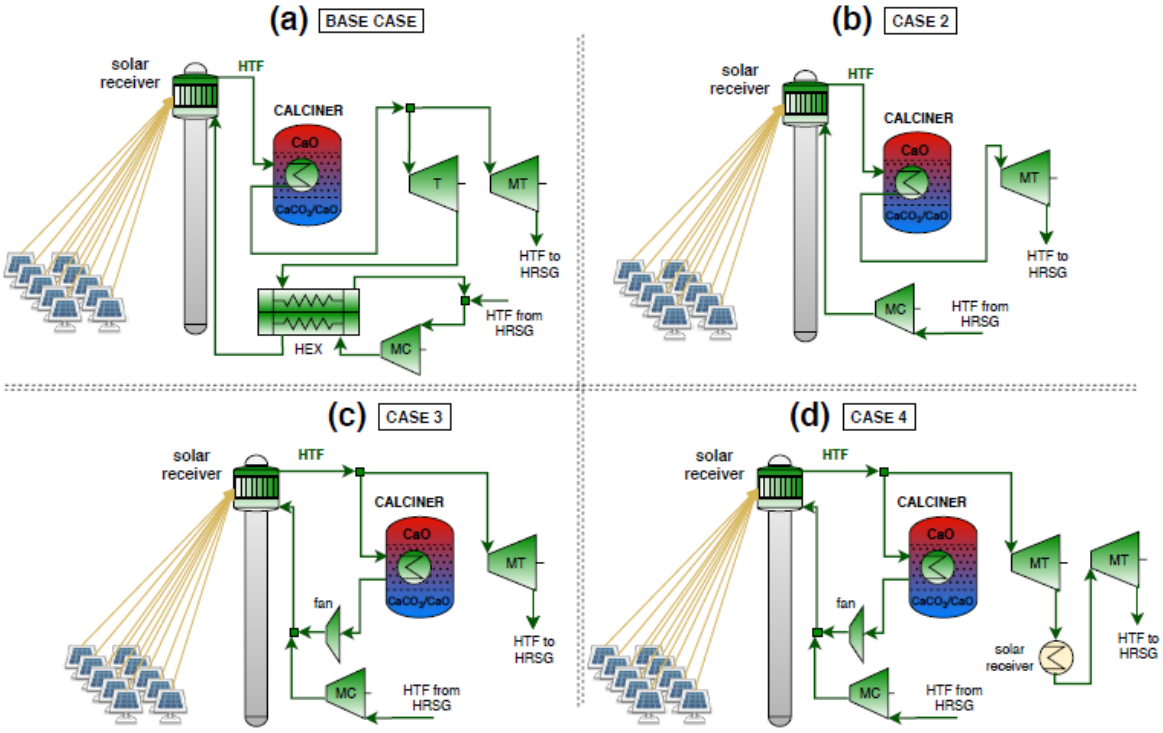

Figure 5: Solar receiver-TCES integration schemes: a) base case configuration with two parallel turbines and recirculating the HFT exiting from one of them; b) sequential HTF stream integration between receiver, calciner and gas turbine; c) high-temperature HTF recirculation to the receiver and d) high-temperature HTF recirculation to the receiver and intermediate reheat in the gas turbine using solar.

Both cases 3 and 4 work under higher pressure (55 and 75 bar respectively) than the base case. While the CO_2 turbomachinery under this PR is not fully developed at large scale, high-pressure heat exchangers could notably improve the economics of the plant because of the notable increase of CO_2 specific heat, conductivity and density at high pressure.

The energy balance for the four proposed configurations is shown in Table 6. The design criterion has been to generate the same power at the main gas turbine (75 MWe) for all configurations, which leads to different thermal power needs at the receiver depending on the configuration. As can be seen, the proposed configurations result in quite different values of the plant efficiency and energy storage capacity. In order to consider the penalty occurring at high SM in comparison with the plant without storage, a sensitivity analysis on the storage capacity has been carried out. The results are illustrated in Figure 6. As can be seen, the sun mode efficiency is notably improved under small energy storage scenarios (less than 8 hours of storage) in cases 3 and 4. However, to increase the dispatchability with a storage capacity higher than 8 hours, the base case provides the best configuration. Note that the design conditions impose storage capacity in case 2 since the SM cannot be modified.

Table 6: 'Day mode' energy balance for several receiver-TCES integrations

	Parameter	'sun mode' (Figure 5)			
		Base case	Case 2	Case 3	Case4
	Solar thermal power (MW_{th})	430.6	187.5	182.51	275.28
HEX (MWth)	HEX	137.6	-	-	-
	CALCINER HE	115.0	37.94	58.96	70.17
	HRSG	73.2	73.2	48.5	73.2
Generation (MWe)	Main HTF turbine (MT)	75.0	75	75	75
	HTF turbine (T2)	152.66	-	-	46.44
	Steam turbine (HPT)	4.87	4.87	3.05	4.87
	Steam turbine (IPT)	9.10	9.1	5.94	9.1
	Steam turbine (LPT)	13.88	13.88	9.23	13.88
Consumption (MWe)	Main HTF Compressor (MC)	-103.02	-33.1	-29.02	-45.23
	CO_2 fan	-	-	-2.64	-3.41
	CO_2 storage compressor (HPC)	-9.56	-3.16	-4.9	-6.33
	Steam cycle pumps (MP, LP, IP, HP)	-0.32	-0.32	-0.21	-0.32
	Cooling pumps/fans	-1.63	-0.88	-0.67	-1.05
	Miscellaneous auxiliaries	-2.64	-1.13	-0.92	-1.46
	Generators losses	-2.85	-1.31	-1.12	-2.68
	W_{net} (MWe)	**135.49**	**62.95**	**53.74**	**88.81**
	"Sun" mode efficiency (charging step)	**31.48%**	**33.57%**	**29.44%**	**32.26%**
	Storage hours	**12**	**4**	**6**	**8**

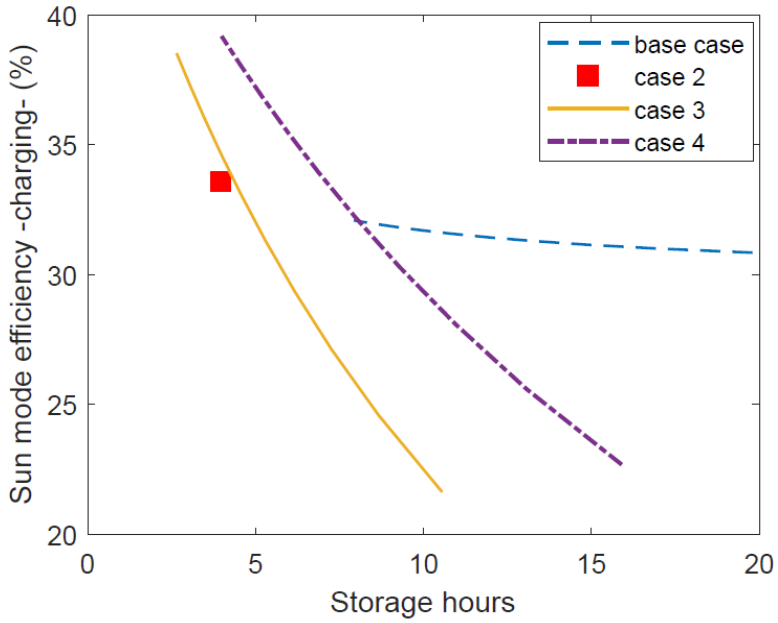

Figure 6: Sun operation mode efficiency as a function of the storage capacity.

As shown in this section, all the proposed cases present advantages and disadvantages depending on the storage requirement of the plant (such as peak-load, baseload, and others). The energy storage density associated to the different process schemes is similar since energy storage conditions and CaO conversion are independent of the receiver-calciner configuration [33]. Regarding maturity, capital cost and ease of implementation, case 2 is clearly the best option since turbomachinery is the same than in a typical CC and no additional heat exchanger is needed. However, the energy storage capacity is limited to 4h of full operation (Figure 6), which casts doubts on the interest and viability of developing a new high-temperature solar receiver and its integration with a TCES just to store such a small amount of energy. Case 4 is the most efficient option, even operating a fan with a high energy consumption due to the high temperature. The systems are somewhat more complicated than the base case due to the need to provide an extra reheat in the receiver, although the lower heat input required for the HFT entering the calciner (275 MWth instead of 430 MWth in the base case) would compensate this issue without apparently affecting the size of the reactor, and therefore cost and radiation losses. More in depth off-design simulations of the plant should be performed to single out the best configuration under a real scenario. An exergo-economic analysis is also pending in order to quantify the impact of the exergy destruction in each process scheme.

4.2 Effect of the Heat Transfer Fluid (HTF)

While CO_2 has been chosen as HTF circulating through the combined cycle, air or Helium are possible alternatives. Using air as HTF is a mature and efficient option, which is the basis of both commercial combined cycles [58] and pressurised solar gas receivers [40]. Air is cheap and freezing or overheating problems are avoided. Moreover, in the case of hybridising the HTSSCC with natural gas, air allows direct combustion in the chamber, without a heat exchanger integration, which leads to higher efficiency than in indirect heating cases. The use of Helium has been proposed as an alternative in closed Brayton cycles [59], although the development of this technology is still far from the commercial stage. Figure 7 shows the different behaviours for the power block efficiency when using air, He and CO_2 as HTF under the base case at design conditions.

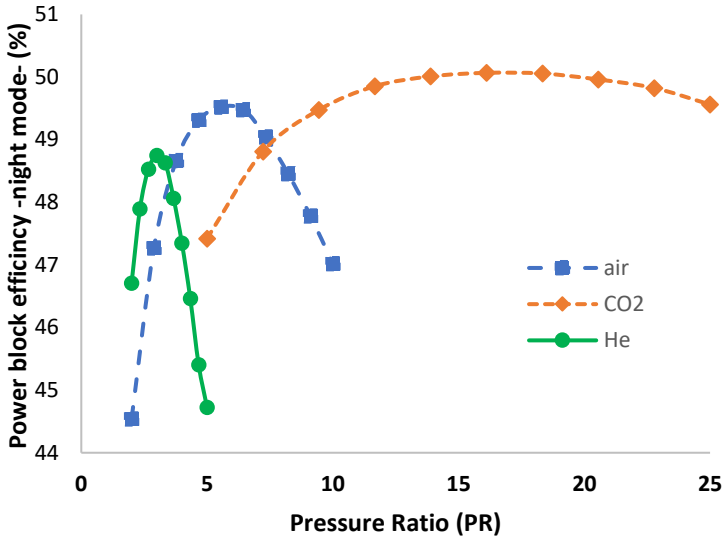

Figure 7: Combined cycle efficiency (night operation mode) as a function of the PR when using Helium, CO_2 and air as heat transfer fluids. Near-to-atmospheric pressure is considered at the turbine outlet.

For the base case, subcritical CO_2 is chosen as HTF because of its higher heat capacity, thermal conductivity, and density compared to compressed air, which leads to a potentially higher thermal receiver efficiency. Similarly, indirect heat transfer in the CFB reactors (TCES) would be enhanced by using CO_2 as HTF. Helium has a notably higher conductivity than air and CO_2, but also a lower density, which requires a remarkably more significant solar receiver to manage the typical large HTF mass flow in combined cycles. The advantages of a more compact solar receiver and heat exchangers by using CO_2 as HTF are even higher for supercritical CO_2 cycles [60], although the technology is still under the non-commercial stage.

As shown in Figure 7, there is not a significant difference between the maximum combined cycle efficiency achieved at the design point when using each one of the possible gases as HTF. Thus, the maximum efficiencies under night operation mode (for a TIT od 1000ºC) when using air, CO_2 and He are 49.5%, 50.1% and 48.8%, respectively. However, there is a difference between the optimum PR to achieve this maximum efficiency due to the different thermodynamic properties of these fluids under optimum operation (Table 7).

Table 7: Thermodynamic properties under optimum PR conditions for air, He and CO2.

Property	Air (1000ºC, 5.5 bar)	He (1000ºC, 3 bar)	CO_2 (1000ºC, 16 bar)
Specific heat [kJ/kg·K]	1.185	**5.193**	1.295
Density [kg/m^3]	1.503	0.113	**6.63**
Conductivity [W/m·K]	0.081	**0.427**	0.088
Viscosity [kg/(m·s)]	5.06 x10^{-5}	5.48 x10^{-5}	4.87 x10^{-5}

Helium provides excellent specific heat and conductivity in comparison with air and CO_2, which leads to a higher efficiency of heat transfer. On the other hand, from a receiver design perspective, the higher the HTF density, the smaller size to manage a certain amount of HTF

mass flow. Despite a detailed cavity receiver design that must be developed to draw further conclusions about the performance of these fluids, from a purely thermodynamic point of view, using CO_2 seems the most convenient choice.

4.3 Sensitivity analysis

A sensitivity analysis has been carried out to evaluate the effects of several key parameters whose values were assumed in Table 3. The results are represented in Figure 8. The most influential parameter is the CO_2 turbomachinery efficiency, as was shown in other CSP-CaL integrations [33] while the pressure losses along the cycle play a minor role.

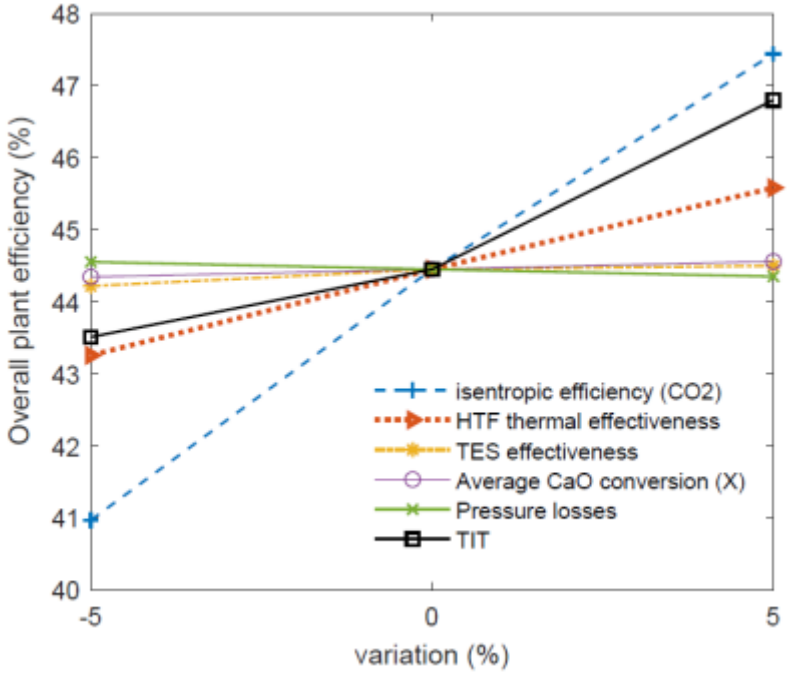

Figure 8: Sensitivity analysis on overall plant efficiency for selected parameters

Unlike other works in which the average CaO conversion of CaO (X) took a fundamental role in the overall process efficiency [53], in the case of the concept proposed in this work, its relevancy is minimal. This can be explained since the most substantial impact on the plant efficiency is due to a higher amount of solids to be recirculated by decreasing the average CaO conversion, which it is associated to solids conveying cost (~10 MJ/tonne/100 m) [4] and the higher amount of thermal power required to preheat the materials up to the temperature of the reactor. However, in the proposed concept there is a minimum solids-conveying cost since solids are fluidised between the CFB reactor, and there are no solid-gas or solid-solid heat exchangers, as well as no need to introduce/extract solids to/from storage silos. Besides, the small temperature difference between reactors minimises the role of the sensible heat to be recovered/provided to the solids streams, and therefore the impact of a higher solids stream over the plant performance is reduced [13]. However, a lower CaO conversion does notably affects other aspects not directly related to the efficiency, as larger plant equipment [13]. Thus, a higher average CaO conversion always takes a positive impact on the plant.

An improved heat transfer in the reactors and the TES system leads to a higher overall efficiency. On the other hand, by increasing the TIT enhance notably the overall plant efficiency. Note that the HTF temperature difference between calciner inlet/outlet is kept as 200ºC as in the base case with the aim of not modifying the SM, which already influences the plant performance as shown in section 4.1.

5. Conclusions

In this paper, a novel High-Temperature Storage Solar Combined Cycle has been presented and simulated at design conditions. By integrating an efficient TCES system, the combined cycle can operate at full load from the solar energy stored, theoretically without any fuel input. Thus, the solar-based plant capacity is notably enhanced in comparison with current ISCC plants, allowing for an efficient operation of the combined cycle with a significantly higher solar share (ideally 100%). In contrast with previous works on TCES and high-temperature CSP systems based on the use of solids, the solar receiver proposed is a pressurised gas cavity instead of a particle receiver, which is a significant challenge for the deployment of gas/solids based TCES systems.

The HTSSCC base case analysed leads to an overall plant efficiency of 44.5%, which is several points higher than the efficiency reported in previous works regarding the CSP-TCES integration based on CO_2 Closed Brayton cycles or steam Rankine cycles. The power block efficiency is over 50% at night whilst its efficiency is penalised under sun hours up to ~30% due to the energy consumed for storage charging. The isentropic efficiency of the turbine has been identified as the main parameter affecting the plant performance, while the loss of CaO activity with the numer of cycles is not so crucial under the high-temperature storage integration proposed. The configuration of the solar receiver-calciner has been found fundamental to determine the amount of energy storable. Thus, by circulating the HTF stream sequentially through the receiver, calciner and power block, the maximum capacity of the storage system would be such that the system could operate at full load for 4 hours in the absence of sun. The energy storage capacity could be increased beyond 15h of storage by using two parallel turbines and by recirculating the hot flow (600ºC) to the solar receiver at the outlet of one of them.

The proposed integration can also be designed with pressurised He or air as HTF and with a maximum temperature in the receiver of 1000ºC. The latter case was successfully tested in previous research projects at the MW scale. Without going into further details that are outside the scope of this work and attending only to a purely thermodynamic point of view, using CO_2 seems the most convenient choice.

Abbreviations

CaL	Calcium-Looping
CC	Combined Cycle
CFB	Circulated Fluidised Bed
CSP	Concentrating Solar Power
DSG	Direct Steam Generation
HTF	Heat Transfer Fluid
HTSSCC	High Temperature Storage Solar Combined Cycle
HRSG	Heat Recovery Steam Generator
ISCC	Integrated Solar Combined Cycles
PR	Pressure Ratio
SM	Solar Multiple
TCES	Thermochemical Energy Storage
TES	Thermal Energy Storage
TIT	Turbine Inlet Temperature

Acknowledgments

The research leading to these results has received funding from the European 'Union's Horizon 2020 research and innovation programme under grant agreement No 727348, project SOCRATCES and by the Spanish Government Agency Ministerio de Economía y Competitividad (MINECO-FEDER funds) under contracts CTQ2017- 83602-C2 (-1-R and -2-R).

Annexes

Table A1: Stream data for the base case (see figure below)

	'sun' mode				'night' mode		
stream id	materials	P (bar)	T(ºC)	m (kg/s)	P (bar)	T(ºC)	m (kg/s)
s1	CO_2 (HTF)	18.75	1200	438.3	-	-	-
s2a	CO_2 (HTF)	18.75	1200	438.3	-	-	-
s2b	CO_2 (HTF)	-	-	-	18.7	413.6	144.5
s3a	CO_2 (HTF)	18.38	1000	438.3	-	-	-
s3b	CO_2 (HTF)	-	-	-	18.33	1000	144.6
s4	CO_2 (HTF)	18.33	1000	144.6	18.33	1000	144.6
s5	CO_2 (HTF)	18.33	1000	293.7	-	-	-
s6a	CO_2 (HTF)	1.02	580.3	144.6	1.02	580.3	144.6
s6b	CO_2 (HTF)	1.02	452.7	144.6	1.02	452.7	144.6
s6c	CO_2 (HTF)	1.01	323.9	144.6	1.01	323.9	144.6
s6d	CO_2 (HTF)	1.01	281.2	144.6	1.01	281.2	144.6
s6e	CO_2 (HTF)	1.01	279	144.6	1.01	279	144.6
s6f	CO_2 (HTF)	1.01	277	144.6	1.01	277	144.6
s6g	CO_2 (HTF)	1.01	237.8	144.6	1.01	237.8	144.6
s6h	CO_2 (HTF)	1.00	175.6	144.6	1.00	175.6	144.6
s6i	CO_2 (HTF)	1.00	158.8	144.6	1.00	158.8	144.6
s7a	CO_2 (HTF)	1.01	579	293.7	-	-	-
s7b	CO_2 (HTF)	1.00	104.3	144.6	1.00	104.3	144.6
s8a	CO_2 (HTF)	1.00	143.3	293.7	-	-	-
s9	CO_2 (HTF)	1.00	130.6	438.3	1.00	104.2	144.5
s10	CO_2 (HTF)	19.32	116.9	438.3	-	-	-
s11	CO_2 (HTF)	1.12	413	438.3	-	-	-
s12	CO_2 (HTF)	-	-	-	18.7	413.6	144.5
p1	CaO	1.00	950.0	275.67	-	-	-
p2	$CaCO_3$/CaO	-	-	-	1.00	1000	308.12
c1	CO_2	1.00	950.0	32.45	-	-	-
c2	CO_2	1.00	35.0	32.45	-	-	-
c3	CO_2	75.75	117.0	32.45	-	-	-
c4	CO_2	75.00	25.0	32.45	-	-	-
c5	CO_2	-	-	-	75.00	25	32.45
c6	CO_2	-	-	-	74.75	100	32.45
c7	CO_2	-	-	-	8.05	100	32.45
c8	CO_2	-	-	-	8	939.0	32.45
h1	steam	108.21	124.2	16.10	108.21	124.2	16.10
h2	steam	106.1	232.2	15.78	106.1	232.2	15.78
h3	steam	104	311.9	15.78	104	311.9	15.78
h4	steam	104	313.9	15.63	104	313.9	15.63
h5	steam	101.97	565	15.49	101.97	565	15.49
i1	steam	27.41	122.3	3.24	27.41	122.3	3.24
i2	steam	26.87	226.7	3.24	26.87	226.7	3.24
i3	steam	26.87	227.8	3.21	26.87	227.8	3.21
i4	steam	25.35	260	3.21	25.35	260	3.21
i5	steam	25.35	353.9	18.46	25.35	353.9	18.46
i6	steam	24.86	565	18.46	24.86	565	18.46
l1	steam	4.6	121.8	1.04	4.6	121.8	1.04
l2	steam	4.6	148.8	1.03	4.6	148.8	1.03
l3	steam	4.34	260	1.03	4.34	260	1.03
l4	steam	4.14	312.9	18.87	4.14	312.9	18.87
l5	steam	4.14	310.1	19.9	4.14	310.1	19.9
l6	steam	0.05	32.9	20.02	0.05	32.9	20.02
l7	steam	0.05	31.79	20.02	0.05	31.79	20.02
l8	steam	3.36	31.66	20.24	3.36	31.66	20.24
l9	steam	3.30	118.3	20.24	3.30	118.3	20.24
l10	steam	3.30	121.8	20.37	3.30	121.8	20.37

References

[1] European Solar Thermal Electricity Association (ESTELA). Solar Thermal Electricity Strategic research agenda 2020-2025 2012.

[2] Conlon WM. Dispatchable solar combined cycle. ASME 2017 11th Int Conf Energy Sustain ES 2017, Collocated with ASME 2017 Power Conf Jt with ICOPE 2017, ASME 2017 15th Int Conf Fuel Cell Sci Eng Technol ASME 201 2017:1–7. https://doi.org/10.1115/ES2017-3578.

[3] Carrillo AJ, Joségonzaíez-Aguilar J, Romero M, Coronado JM. Solar Energy on Demand: A Review on High Temperature Thermochemical Heat Storage Systems and Materials 2017. https://doi.org/10.1021/acs.chemrev.8b00315.

[4] Chacartegui R, Alovisio A, Ortiz C, Valverde JMM, Verda V, Becerra JAA. Thermochemical energy storage of concentrated solar power by integration of the calcium looping process and a CO2 power cycle. Appl Energy 2016;173:589–605. https://doi.org/10.1016/j.apenergy.2016.04.053.

[5] Bagherisereshki E, Tran J, Lei F, AuYeung N. Investigation into SrO/SrCO 3 for high temperature thermochemical energy storage. Sol Energy 2018;160:85–93. https://doi.org/10.1016/j.solener.2017.11.073.

[6] Qu X, Li Y, Li P, Wan Q, Zhai F. The development of metal hydrides using as concentrating solar thermal storage materials. Front Mater Sci 2015;9:317–31. https://doi.org/10.1007/s11706-015-0311-y.

[7] Schmidt M, Linder M. Power generation based on the Ca(OH)2/ CaO thermochemical storage system – Experimental investigation of discharge operation modes in lab scale and corresponding conceptual process design. Appl Energy 2017;203:594–607. https://doi.org/10.1016/j.apenergy.2017.06.063.

[8] Flegkas S, Birkelbach F, Winter F, Freiberger N, Werner A. Fluidized bed reactors for solid-gas thermochemical energy storage concepts - Modelling and process limitations. Energy 2018;143:615–23. https://doi.org/10.1016/j.energy.2017.11.065.

[9] Block T, Schmücker M. Metal oxides for thermochemical energy storage: A comparison of several metal oxide systems. Sol Energy 2016;126:195–207. https://doi.org/10.1016/j.solener.2015.12.032.

[10] Edwards JH, Do KT, Maitra a. M, Schuck S, Fok W, Stein W. The use of solar-based CO2/CH4 reforming for reducing greenhouse gas emissions during the generation of electricity and process heat. Energy Convers Manag 1996;37:1339–44. https://doi.org/10.1016/0196-8904(95)00343-6.

[11] Masci G, Ortiz C, Chacartegui R, Verda V, Jose M. The Ammonia Looping System for Mid-Temperature Thermochemical Energy Storage 2018;70:763–8. https://doi.org/10.3303/CET1870128.

[12] Sattler C, Roeb M, Agrafiotis C, Thomey D. Solar hydrogen production via sulphur based thermochemical water-splitting. Sol Energy 2017;156:30–47. https://doi.org/10.1016/j.solener.2017.05.060.

[13] Ortiz C, Valverde JM, Chacartegui R, Perez-Maqueda LA, Giménez P. The Calcium-Looping (CaCO3/CaO) process for thermochemical energy storage in Concentrating Solar Power plants. Renew Sustain Energy Rev 2019;113:109252. https://doi.org/10.1016/j.rser.2019.109252.

[14] SOCRATCES project Consortium. Socratces Project 2018. https://socratces.eu/.

[15] Ortiz C, Manuel Valverde J, Chacartegui R, Pérez-Maqueda LA, Gimenez-Gavarrell P. Scaling-up the Calcium-Looping Process for CO_2 Capture and Energy Storage. KONA Powder Part J 2021:1–20. https://doi.org/10.14356/kona.2021005.

[16] Barker R. The reactivity of calcium oxide towards carbon dioxide and its use for energy storage. J Appl Chem Biotechnol 1974;24:221–7. https://doi.org/10.1002/jctb.2720240405.
[17] Valverde JM, Barea-López M, Perejón A, Sánchez-Jiménez PE, Pérez-Maqueda LA. Effect of Thermal Pretreatment and Nanosilica Addition on Limestone Performance at Calcium-Looping Conditions for Thermochemical Energy Storage of Concentrated Solar Power. Energy and Fuels 2017;31:4226–36. https://doi.org/10.1021/acs.energyfuels.6b03364.
[18] Zhai R, Li C, Qi J, Yang Y. Thermodynamic analysis of CO2capture by calcium looping process driven by coal and concentrated solar power. Energy Convers Manag 2016;117:251–63. https://doi.org/10.1016/j.enconman.2016.03.022.
[19] Tregambi C, Montagnaro F, Salatino P, Solimene R. A model of integrated calcium looping for CO<inf>2</inf> capture and concentrated solar power. Sol Energy 2015;120:208–20. https://doi.org/10.1016/j.solener.2015.07.017.
[20] Ortiz C, Chacartegui R, Valverde JMM, Alovisio A, Becerra JAA. Power cycles integration in concentrated solar power plants with energy storage based on calcium looping. Energy Convers Manag 2017;149:815–29. https://doi.org/10.1016/j.enconman.2017.03.029.
[21] Tesio U, Guelpa E, Verda V. Integration of thermochemical energy storage in concentrated solar power. Part 1: Energy and economic analysis/optimization. Energy Convers Manag X 2020;6:100039. https://doi.org/10.1016/j.ecmx.2020.100039.
[22] Khandelwal N, Sharma M, Singh O, Shukla AK. Recent Developments in Integrated Solar Combined Cycle Power Plants. J Therm Sci 2020;29:298–322. https://doi.org/10.1007/s11630-020-1278-2.
[23] Kelly Bruce, Herrmann U, Hale MJ. Optimization studies for integrated solar combined cycles, 2001.
[24] Rovira A, Montes MJ, Varela F, Gil M. Comparison of Heat Transfer Fluid and Direct Steam Generation technologies for Integrated Solar Combined Cycles. Appl Therm Eng 2013;52:264–74. https://doi.org/10.1016/j.applthermaleng.2012.12.008.
[25] Li Y, Yang Y. Thermodynamic analysis of a novel integrated solar combined cycle. Appl Energy 2014;122:133–42. https://doi.org/10.1016/j.apenergy.2014.02.017.
[26] Montes MJ, Rovira A, Muñoz M, Martínez-val JM. Performance analysis of an Integrated Solar Combined Cycle using Direct Steam Generation in parabolic trough collectors. Appl Energy 2011;88:3228–38. https://doi.org/10.1016/j.apenergy.2011.03.038.
[27] Libby C, Golden J, Bedilion R, Turchi C. Assessment of direct steam generation technologies for solar thermal augmented steam cycle applications. Energy Procedia 2014;49:1420–8. https://doi.org/10.1016/j.egypro.2014.03.151.
[28] Korzynietz R, Brioso JA, Del Río A, Quero M, Gallas M, Uhlig R, et al. Solugas - Comprehensive analysis of the solar hybrid Brayton plant. Sol Energy 2016;135:578–89. https://doi.org/10.1016/j.solener.2016.06.020.
[29] Barin I. Thermochemical data of pure substances VCH, Weinheim (1989) 1989.
[30] Valverde JM, Sanchez-Jimenez PE, Perez-Maqueda L. Calcium-looping for post-combustion CO2 capture. On the adverse effect of sorbent regeneration under CO2. Appl Energy 2014;126:161–71. https://doi.org/10.1016/j.apenergy.2014.03.081.
[31] Shimizu T, Hirama T, Hosoda H, Kitano K, Inagaki M, Tejima K. A Twin Fluid-

Bed Reactor for Removal of CO2 from Combustion Processes. Chem Eng Res Des 1999;77:62–8. https://doi.org/10.1205/026387699525882.
[32] Arias B, Diego ME, Abanades JC, Lorenzo M, Diaz L, Martínez D, et al. Demonstration of steady state CO2 capture in a 1.7MWth calcium looping pilot. Int J Greenh Gas Control 2013;18:237–45. https://doi.org/10.1016/j.ijggc.2013.07.014.
[33] Ortiz C, Romano MC, Valverde JM, Binotti M, Chacartegui R. Process integration of Calcium-Looping thermochemical energy storage system in concentrating solar power plants. Energy 2018;155:535–51. https://doi.org/10.1016/j.energy.2018.04.180.
[34] Kim K, Kim D, Park YK, Lee KS. A solid sorbent-based multi-stage fluidized bed process with inter-stage heat integration as an energy efficient carbon capture process. Int J Greenh Gas Control 2014;26:135–46. https://doi.org/10.1016/j.ijggc.2014.03.012.
[35] Astolfi M, De Lena E, Romano MC. Improved flexibility and economics of Calcium Looping power plants by thermochemical energy storage. Int J Greenh Gas Control 2019;83:140–55. https://doi.org/10.1016/j.ijggc.2019.01.023.
[36] Ortega-Fernández I, Calvet N, Gil A, Rodríguez-Aseguinolaza J, Faik A, D'Aguanno B. Thermophysical characterization of a by-product from the steel industry to be used as a sustainable and low-cost thermal energy storage material. Energy 2015;89:601–9. https://doi.org/10.1016/j.energy.2015.05.153.
[37] Ortega I, Faik A, Gil A, Rodríguez-Aseguinolaza J, D'Aguanno B. Thermo-physical Properties of a Steel-making by-product to be used as Thermal Energy Storage Material in a Packed-bed System. Energy Procedia 2015;69:968–77. https://doi.org/10.1016/j.egypro.2015.03.180.
[38] Peng X, Yao M, Root TW, Maravelias CT. Design and Analysis of Concentrating Solar Power Plants with Fixed-bed Reactors for Thermochemical Energy Storage. Appl Energy 2020;262:114543. https://doi.org/10.1016/j.apenergy.2020.114543.
[39] Yang H, Xu Y, Acosta-Iborra A, Santana D. Solar tower enhanced natural draft dry cooling tower. AIP Conf Proc 2017;1850. https://doi.org/10.1063/1.4984393.
[40] Sedighi M, Padilla RV, Taylor RA, Lake M, Izadgoshasb I, Rose A. High-temperature, point-focus, pressurised gas-phase solar receivers: A comprehensive review. Energy Convers Manag 2019;185:678–717. https://doi.org/10.1016/j.enconman.2019.02.020.
[41] National Renewable Energy Laboratory (NREL). Concentrating Solar Power Projects 2017. https://www.nrel.gov/csp/solarpaces/index.cfm (accessed July 1, 2018).
[42] Romeo LM, Bolea I, Lara Y, Escosa JM. Optimization of intercooling compression in CO2capture systems. Appl Therm Eng 2009;29:1744–51. https://doi.org/10.1016/j.applthermaleng.2008.08.010.
[43] Ortiz C, Valverde JM, Chacartegui R, Perez-Maqueda LA. Carbonation of Limestone Derived CaO for Thermochemical Energy Storage: From Kinetics to Process Integration in Concentrating Solar Plants. ACS Sustain Chem Eng 2018;6:6404–17. https://doi.org/10.1021/acssuschemeng.8b00199.
[44] Romano MC. Ultra-high CO2capture efficiency in CFB oxyfuel power plants by calcium looping process for CO2recovery from purification units vent gas. Int J Greenh Gas Control 2013;18:57–67. https://doi.org/10.1016/j.ijggc.2013.07.002.
[45] Perejón A, Miranda-Pizarro J, Pérez-Maqueda LA, Valverde JM. On the relevant role of solids residence time on their CO2 capture performance in the Calcium Looping technology. Energy 2016;113:160–71.

https://doi.org/10.1016/j.energy.2016.07.028.
[46] Valverde JM. On the negative activation energy for limestone calcination at high temperatures nearby equilibrium. Chem Eng Sci 2015;132:169–77. https://doi.org/10.1016/j.ces.2015.04.027.
[47] Schorcht F, Kourti I, Scalet BM, Roudier S, Sancho LD. Best Available Techniques (BAT) Reference Document for the Production of Cement, Lime and Magnesium Oxide. 2013. https://doi.org/10.2788/12850.
[48] Valverde JM, Sanchez-Jimenez PE, Perez-Maqueda L. Role of precalcination and regeneration conditions on postcombustion CO 2 capture in the Ca-looping technology. Appl Energy 2014;136:347–56. https://doi.org/10.1016/j.apenergy.2014.09.052.
[49] Dean CC, Dugwell D, Fennell PS. Investigation into potential synergy between power generation, cement manufacture and CO2 abatement using the calcium looping cycle. Energy Environ Sci 2011;4:2050. https://doi.org/10.1039/c1ee01282g.
[50] Thermoflow Inc. Thermoflex, Fully-flexible design and simulation of conventional steam plants, combined cycles, and other thermal power systems n.d.
[51] Miller JE, Ambrosini A, Babiniec SM, Coker EN, Ho CK, Al-Ansary H, et al. High performance reduction/oxidation metal oxides for thermochemical energy storage (PROMOTES). ASME 2016 10th Int Conf Energy Sustain ES 2016, Collocated with ASME 2016 Power Conf ASME 2016 14th Int Conf Fuel Cell Sci Eng Technol 2016;1:1–8. https://doi.org/10.1115/ES2016-59660.
[52] Sánchez D, Chacartegui R, Muñoz De Escalona JM, Muñoz A, Sánchez T. Performance analysis of a MCFC & supercritical carbon dioxide hybrid cycle under part load operation. Int J Hydrogen Energy 2011;36:10327–36. https://doi.org/10.1016/j.ijhydene.2010.09.072.
[53] Alovisio A, Chacartegui R, Ortiz C, Valverde JM, Verda V. Optimizing the CSP-Calcium Looping integration for Thermochemical Energy Storage. Energy Convers Manag 2017;136:85–98. https://doi.org/10.1016/j.enconman.2016.12.093.
[54] Casati E, Casella F, Colonna P. Design of CSP plants with optimally operated thermal storage. Sol Energy 2015;116:371–87. https://doi.org/10.1016/j.solener.2015.03.048.
[55] International Renewable Energy Agency (IRENA). CSP Charts (IRENA DATABASE) n.d.
[56] Ortiz C, Binotti M, Romano MC, Manuel J. Off-design model of concentrating solar power plant with thermochemical energy storage based on calcium-looping. vol. 210006, 2019, p. 210006. https://doi.org/10.1063/1.5117755.
[57] Quero M, Korzynietz R, Ebert M, Jiménez AA, del Río A, Brioso JA. Solugas – Operation Experience of the First Solar Hybrid Gas Turbine System at MW Scale. Energy Procedia 2014;49:1820–30. https://doi.org/10.1016/j.egypro.2014.03.193.
[58] NETL. Cost and Performance Baseline for Fossil Energy Plants Volume 1a: Bituminous Coal (PC) and Natural Gas to Electricity, Revision 3, vol. DOE/NETL-2015/1723 2015;1.
[59] Wright S a, Vernon ME, Pickard PS. Concept design for a high temperature helium brayton cycle with interstage heating and cooling 2006.
[60] Chacartegui R, Muñoz De Escalona JM, Sánchez D, Monje B, Sánchez T. Alternative cycles based on carbon dioxide for central receiver solar power plants. Appl Therm Eng 2011;31:872–9. https://doi.org/10.1016/j.applthermaleng.2010.11.008.

1
2